

## EFFECTS OF SULFURIZATION TEMPERATURE ON STRUCTURAL, MORPHOLOGICAL, AND OPTOELECTRONIC PROPERTIES OF CTS THIN FILMS SOLAR CELLS

E. S. HOSSAIN<sup>a\*</sup>, P. CHELVANATHAN<sup>b</sup>, S. A. SHAHAMADI<sup>a,c</sup>,  
M. T. FERDAOUS<sup>a</sup>, B. BAIS<sup>a</sup>, S. K. TIONG<sup>c</sup>, N. AMIN<sup>a,c\*</sup>

<sup>a</sup>*Department of Electrical, Electronics and System Engineering, Universiti Kebangsaan Malaysia (UKM), 43600 Bangi, Selangor, Malaysia*

<sup>b</sup>*Solar Energy Research Institute (SERI), Universiti Kebangsaan Malaysia (UKM), 43600 Bangi, Selangor, Malaysia*

<sup>c</sup>*Institute of Sustainable Energy (ISE), Universiti Tenaga Nasional (@The National Energy University), Jalan IKRAM-UNITEN, 43000 Kajang, Selangor, Malaysia*

Cu<sub>2</sub>SnS<sub>3</sub> (CTS) thin films were fabricated by two-step process: deposition of precursor by RF magnetron sputtering, and subsequent sulfurization at different temperatures. The influence of sulfurization temperatures on the structural, morphological, optical, and electrical properties was investigated to find out the optimum growth route for CTS formation kinetics. All prepared samples were found Sn-rich by the EDX compositional analysis. Structural analysis confirmed the CTS formation with the impurity phase of Cu<sub>4</sub>Sn<sub>7</sub>S<sub>16</sub> at lower temperature, and Sn<sub>2</sub>S<sub>3</sub> at higher sulfurization temperature. Crystallite size of these films was found to increase from 53.2 to 61.3 nm with increasing the sulfurization temperatures from 520 to 580 °C. The same trend was also observed for the grain size in the morphological analysis. Bandgap was varied from 0.87 to 0.92 eV, as the sulfurization temperature increased from 520 to 580 °C. Carrier concentration was found to decline with increasing sulfurization temperature while mobility and resistivity showed a progressive increment at higher temperatures.

(Received July 15, 2018; Accepted October 15, 2018)

*Keywords:* Cu<sub>2</sub>SnS<sub>3</sub> thin films, Sputtering, Sulfurization, Structural and optical properties, solar cells.

### 1. Introduction

Cadmium telluride (CdTe) and copper indium gallium selenide (CIGS) based thin film absorbers have achieved world record power conversion efficiency (PCE) of 22.1% and 22.9%, respectively [1]. However, the toxicity (Cd) and usage of rare earth materials (Te, In) are projected to hinder tera-watt scale for commercialization [2]. Copper zinc tin sulfide (CZTS) consist of all earth abundant materials, has been considered as the prominent substitute for CIGS based solar cell. Recently, it has achieved the record PCE of 12.6% for partial selenium substitution [3]. However, for a narrow chemical potential stable region, this absorber layer suffers from formation of impurity phases, thus hampering further improvement of efficiency [4, 5]. Cu<sub>2</sub>SnS<sub>3</sub> (CTS) has come to researchers' attention, as this ternary phase often produced as a byproduct during the fabrication of CZTS. Having similarity in crystal structure of CZTS, CTS has been considered as a prospective candidate for chalcogenide based absorber due to its tunable narrow bandgap (0.9 to 1.35 eV), p-type conductivity with high absorption coefficient ( $>10^4$  cm<sup>-1</sup>) [6-9]. Above all, it entirely consists of earth-abundant and environment friendly components. Moreover, in terms of chemical potential phase space, Cu<sub>2</sub>SnS<sub>3</sub> possesses the broadest stable range in Cu-Sn-S family [10]. Different fabrication methods have been utilized to fabricate CTS based thin film solar cells, including sputtering [11], vacuum evaporation [12, 13], electron beam evaporation [14],

---

\*Corresponding author: nowshad@uniten.edu.my

electrodeposition [15], spray pyrolysis [16], successive ionic layer adsorption and reaction [17], chemical bath deposition [18], and solid reactions [19]. However, the highest PCE (4.63%) for CTS has been reported by co-evaporation method [20], which is still low to initiate rigorous pre-commercial research effort. Moreover, this method is not suitable for large-scale production due to lack of sufficient process stability and homogeneity [21]. In terms of composition control and smooth large-scale production capability, sputtering is the best method. However, the best PCE reported from this method is only 3.05% [22].

Continuous work to identify the optimum growth route to deposit void free and highly crystalline CTS phase is an on-going effort. Sulfurization step is an important stage to control the growth formation kinetics of CTS. However, the overall performance of CTS has not met the satisfactory level so far. One of the possible reasons for this lower efficiency is the poor crystallization and unfavorable morphology of the CTS absorber layer. For an ideal photovoltaic absorber layer, columnar grains growth perpendicular to surface is desirable to suppress the grain boundaries along the horizontal direction, and thus reduce the recombination centers for the minority carriers. Consequently, better crystallinity is necessary for optimum output of CTS solar cells, which can only be achieved by optimized sulfurization of as-deposited precursor films. Sulfurization is a variant of post-deposition annealing process, which is normally done in closed space in the presence of sulfur source and a suitable working gas ( $N_2$  or Argon) [23]. Several parameters of sulfurization such as temperature, holding time, working pressure, temperature ramp rate, and sulfur content have different impacts on quality of CTS film.

However, the most important parameter, which controls the growth formation kinetics of CTS is temperature. In the literature, it has been found that this parameter controls the phase of CTS, in which at high temperature ( $>775\text{ }^\circ\text{C}$ ) the cubic structure forms whereas at low temperature ( $<775\text{ }^\circ\text{C}$ ) stable monoclinic phase forms [24-26]. There are several reports regarding the effects of sulfurization temperature variations on CTS thin film absorber layer [7, 11, 27, 28]. However, in-depth analysis is needed to understand the exact material properties as well as the growth formation kinetics of CTS thin film. Recently, P. Guan et.al reported a DFT analysis about CTS optimum growth conditions and proposed a two-step sulfurization profile for CTS absorber [29]. In this report, the authors suggest to maintain lower temperature below  $400\text{ }^\circ\text{C}$  for the formation of CTS phase, and higher temperature more than  $500\text{ }^\circ\text{C}$  for better crystallinity and bigger grain size. Hence, the proposed two-step sulfurization has been carried out to investigate the effects of the temperature variations on the structural, morphological, optical, and electrical characteristics of CTS thin films.

## 2. Experimental details

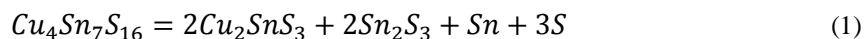
Soda lime glass (SLG) substrates were sequentially ultrasonically cleaned by methanol-acetone-methanol-deionized water sequence, and then dried by  $N_2$  gas flow. Back contact metal was deposited by magnetron sputtering using a 2-in Mo target (purity of 99.95%) on the SLG substrates [30, 31]. The stacked metallic precursors were sequentially deposited by using radio frequency (RF) sputtering on Mo-coated SLG from Sn target (5N), and then from copper-tin alloy (CT) target (purity of 99.99% with the composition of 65% Cu, and 35% Sn). Additional Sn content is to ensure the composition of fabricated samples to be in Cu-poor condition. In both cases, the deposition was carried out in high purity argon atmosphere, with a base pressure of  $6\times 10^{-6}$  Torr at room temperature (RT). The sputtering power of Sn and CT target was set to 80 W, and 50 W, respectively, whereas argon flow was fixed at 4 SCCM. After preheating the Mo-coated substrates at  $100\text{ }^\circ\text{C}$  for 40 min, the Sn, and CT targets were sequentially deposited for 30, and 60 min, respectively at the working pressure of 20 mTorr. This lower substrate heating temperature is useful to assist the interdiffusion of metal elements, which in turn enhances the uniformity, density, and morphological properties of films [32-35]. Sulfurization was carried out in a tube furnace by putting the samples in a graphite box with 120 mg sulfur powder, and 20 mg SnS powder [36]. Prior to sulfurization, purging was done to ensure a contamination free environment. Two-step sulfurization was applied with a base pressure of 90 mTorr, and working

pressure of 200 Torr at RT. Temperature was increased with a rate of 5 °C/min, and the holding time for the lower temperature at 350 °C was kept fixed for 30 min, meanwhile holding time for the higher temperature at 520 °C, 550 °C, and 580 °C was fixed for 60 min. The samples fabricated at 520 °C, 550 °C, and 580 °C have been marked as T1, T2, and T3. For structural and crystallographic analysis of sulfurized CTS absorber, X-ray diffraction (XRD) was done using BRUKER AXS-D8 advance at RT. The XRD patterns were captured with Cu-K $\alpha$  radiation ( $\lambda = 1.5408 \text{ \AA}$ ) in the  $2\theta$  range from 20° to 80° with a step size of 0.02°. Morphological analysis was done by using Hitachi SU1510 scanning electron microscopy (SEM), which was operated at 3 kV to 15 kV. Compositional measurement was carried out through using Horiba EMAX 450 energy-dispersive X-ray (EDX) spectroscopy at 300x magnification (spot size 1mm  $\times$  1 mm), and accelerating voltage of 15 kV. Optical property explicitly bandgap was estimated from reflectance measurement by using Perkin-Elmer Lambda 950 UV/VIS/NIR spectrometer, which was equipped with a 60 mm integrating sphere from 190 to 2500 nm. HMS ECOPIA 3000 system was used to measure the electrical properties of CTS like carrier concentration, mobility, and resistivity with a magnetic field of 0.57 T, and probe current of 10  $\mu$ A.

### 3. Result and discussion

#### 3.1. Structural and crystallographic analysis

Fig. 1 shows the XRD patterns obtained for the samples sulfurized at 520 °C, 550 °C, and 580 °C, which are marked as T1, T2, and T3, respectively. According to the diffraction patterns, all films are found to possess a strong peak at 28.3° with a preferential orientation of (-131) as well as three weak peaks located at 32.65°, 47.2°, and 55.85°. These detected patterns are similar to either a monoclinic phase (JCPD card no. 01-072-9611) or a cubic phase (JCPD card no. 01-089-2877). The reported formation temperature of cubic phase has been found more than 775 °C [24, 25], which is quite higher than our sulfurization temperatures. Consequently, observed patterns can be acknowledged as the monoclinic crystal structure, which is in agreement with U. Chalapathi et al. correspondingly [37]. Moreover, the existence of two secondary phases is observed, which are explained as follows. The first secondary phase is associated with  $\text{Cu}_4\text{Sn}_7\text{S}_{16}$  that can be traced to JCPD card no. 01-089-4713. This secondary phase shows the dominating peak located at 34.16° with an orientation plane of (200). As shown, patterns related to this secondary phase remain almost persistent at 520 and 550 °C, and as the temperature increases to 580 °C, this secondary phase diminishes along with all peaks except for 24.34°, 37.74°, and 49.27° peaks. This observation indicates that some portions of this secondary phase are still existent in the sample T3. Another secondary phase,  $\text{Sn}_2\text{S}_3$  (JCPD card no. 01-075-2183) is found only at the sulfurization temperature of 550 and 580 °C. At 550 °C, the formation of  $\text{Sn}_2\text{S}_3$  starts and two peaks located at 21.34°, and 31.62° are detected. However, results indicate the higher sulfurization temperature stimulates the  $\text{Cu}_4\text{Sn}_7\text{S}_{16}$  component to break into CTS and  $\text{Sn}_2\text{S}_3$  (shown in Eqn. 1), which leads into the presence of many  $\text{Sn}_2\text{S}_3$  peaks at 580 °C.



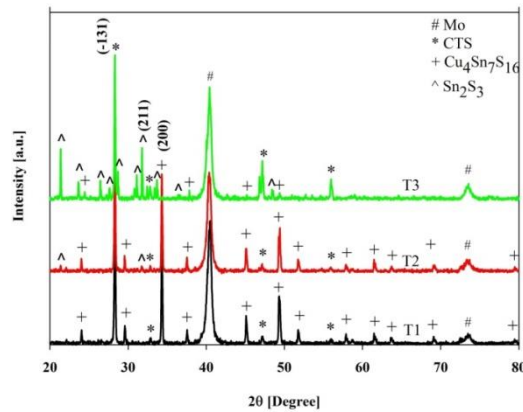


Fig. 1. XRD patterns of the samples sulfurized at different temperatures.

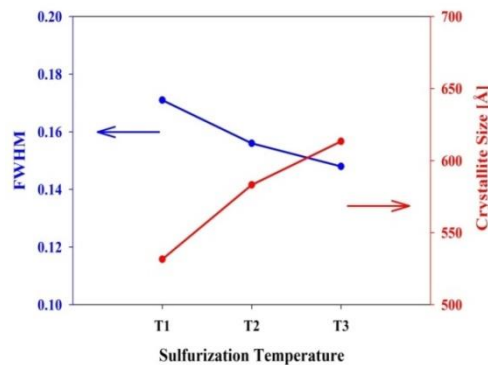


Fig. 2. Variations of FWHM and crystallite size of CTS samples for different sulfurization temperatures

A comparison of full width half-maximum (FWHM) is shown in Fig. 2 for the main peak of CTS oriented as (-131) plane. From the figure, the measured FWHM values are 0.171, 0.156, and 0.148 for samples T1, T2, and T3, respectively. The crystallite size, which was calculated using Scherer's equation, is linearly increasing with the temperature increment, from 53.15 nm for 520 °C to 61.34 nm for 580 °C. Therefore, from the structural point of view, higher sulfurization temperature has been found to be favorable for better crystallinity of CTS thin films.

### 3.2. Compositional analysis

Table 1 shows the elemental compositions for the CTS films prepared at different sulfurization temperatures. To keep all sulfurized films in Sn-rich condition, we intentionally made the precursor (denoted as P) composition more Sn-rich by adding further elemental Sn with the single target CT, which is described in experimental section. As shown, the composition ratio of Cu/Sn for deposited sample is found 1.053 that changes to 1.072 at 520 °C. As the sulfurization temperature increases further, the Cu/Sn ratio changes to 1.148 at 550 °C, and finally, 1.525 at 580 °C. The increment of Cu/Sn ratio with temperature can be attributed to the amount of Sn-loss during sulfurization, which is more at higher temperature. From XRD analysis, it has shown that as the temperature crosses over 550 °C, Sn-rich  $\text{Cu}_4\text{Sn}_7\text{S}_{16}$  breaks into CTS,  $\text{Sn}_2\text{S}_3$ , Sn, and S. These elemental Sn, and S may form the volatile SnS inside the graphite box and evaporated, which causes significant increment of Cu/Sn ratio at 580 °C. The evaporation of S also causes gradual decrement of the S/metal ratio up to 0.982 at 580 °C. The closer to unity value of S/metals also indicates the completion of sulfurization process at 580 °C [7].

Table 1. Compositional analysis of CTS thin films sulfurized at different temperatures.

Sample ID	Elemental percentage (atomic)			Compositional ratio	
	Cu	Sn	S	Cu/Sn	S/metals
P	51.29	48.71	N/A	1.053	N/A
T1	23.59	22.01	54.4	1.072	1.193
T2	25.04	21.81	53.15	1.148	1.135
T3	30.47	19.98	49.55	1.525	0.982

### 3.3. Morphological analysis

Surface morphology of samples is demonstrated in Fig. 3 to investigate the effect of sulfurization temperatures on the deposited precursor P. As shown, the sample T1 appears to contain huge agglomerations on its surface in the form of a number of small grains, and as a result higher grain boundaries. As the temperature increases, grain enlargement can be observed due to coalescence process. The grain size shows its optimum value at the highest sulfurization temperature of 580 °C, which also agrees well with the XRD result. However, some agglomerations are still present on the surface of T3, which might indicate the necessity of more sulfurization time to convert all these agglomerations into larger grains. However, the presence of pinholes is insignificant compared to Sn and S loss in sample T3, which can be attributed to the enhanced crystallinity and larger grain size. From the morphological point of view, sulfurization temperature has a great impact, and higher temperature has proven to produce better crystalline CTS absorber layer.

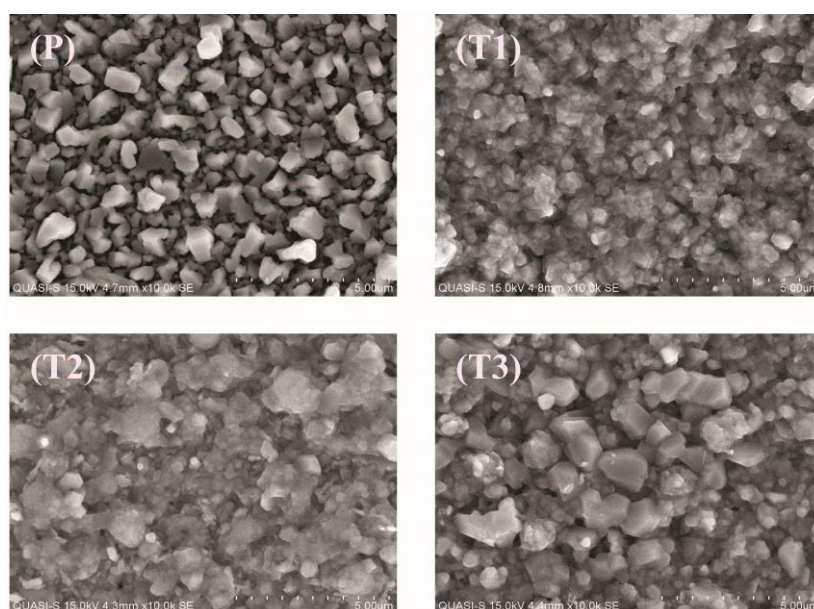


Fig. 3. Surface morphology of precursor and sulfurized CTS thin films.

### 3.4. Optical bandgap measurement

Reflectance was measured to determine the direct bandgap of CTS samples fabricated at different sulfurization temperatures. Kubelka-Munk function was applied to calculate the bandgap using the measured reflectance. According to Kubelka-Munk function theory,  $F$  is calculated by  $(1-R)^2/2R$ , and for direct bandgap absorber,  $Fh\nu \propto (h\nu - E_g)^{1/2}$ , where  $\nu$  is the frequency of photon,  $h$  is the Planck's constant, and  $E_g$  is the bandgap [38]. As shown in Fig. 4, the bandgap is calculated by extrapolating the linear portion of the curve to the horizontal axis. Using this technique, the direct bandgap is estimated to be 0.87 eV for the sample T1, which is increased to 0.91 eV for T2, and 0.92 eV for T3. Therefore, higher sulfurization temperature has been found to enhance the direct bandgap of CTS thin films, which is favorable for higher open circuit voltage, and thus better efficiency. Estimated bandgap values in this study are justified with the previous reported value for monoclinic CTS phase [25, 39-41].

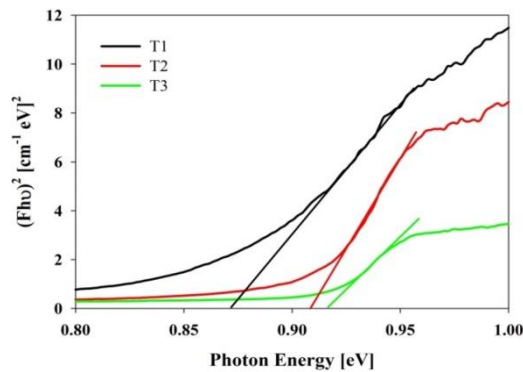


Fig. 4. Estimation of bandgap for fabricated different CTS thin films using Kubelka-Munk function.

### 3.5. Electrical properties

Table 2 summarizes the hall measurement data to investigate the effect of temperature on the electrical properties of sulfurized CTS thin films. The measured carrier concentration of sample T1 is  $1.11 \times 10^{18}$ , which decreases to  $5.09 \times 10^{17}$  and  $1.11 \times 10^{17}$  for samples T2 and T3, respectively. The fabricated CTS films in this study are not intentionally doped, and the observed carrier concentration is introduced by defect states, which are originated from the deviations of ideal elemental stoichiometry [27]. As EDX result suggested that the sample T1 and T2 are Cu-poor and S-rich therefore, S interstitials ( $S_1$ ), Cu vacancies ( $V_{Cu}$ ), and Sn atoms in Cu sites ( $Sn_{Cu}$ ) are the probable defect states. Among them,  $S_1$  and  $V_{Cu}$  are acceptor defect states and  $Sn_{Cu}$  is donor defect states. According to hall measurement, all samples were found to have p-type conductivity, thus the effective defect states are mostly  $S_1$  and  $V_{Cu}$ . However, for T3 the origin of carrier concentration would be dominated by  $V_{Cu}$ , since  $S_1$  is absent here due to sulfur deficiency. The amount of  $V_{Cu}$  is linearly related to the degree of Cu-poor level as well. Moreover, the Cu/Sn ratio was seen to increase by temperature, which eventually decreases the  $V_{Cu}$  defect states. The above analysis signifies the decreasing trend of carrier concentration with increasing sulfurization temperature. According to our theoretical analysis regarding the relationship between carrier concentration and space charge region of CTS, the optimum carrier concentration of CTS was reported in the range of  $10^{16} \text{ cm}^{-3}$  [42], which matches with the result of T3 most.

It was reported that the defect states of  $V_{Cu}$  and  $S_I$  are responsible for the formation of acceptor impurity band in the forbidden band. Due to presence of this acceptor impurity band, the impurity band mobility ( $\mu_i$ ) and the valence band hole mobility ( $\mu_v$ ) can be related to the films mobility ( $\mu$ ) [43]. The  $\mu_v$  can be related to the ionized impurities scattering, acoustic-lattice modes, optical-lattice modes, neutral impurities, and space-charge effects etc. As a function of temperature, decreasing trend of  $\mu_v$  with temperature is related to the effects of acoustic phonon scattering, whereas increasing tendency of  $\mu_v$  can be related to the scattering by the ionized impurities [44]. In our study, the mobility of films decreases from 1.14  $\text{cm}^2/\text{Vs}$  to 1.07  $\text{cm}^2/\text{Vs}$  as the temperature changes from 520 °C to 550 °C. However, this value increases to 3.60  $\text{cm}^2/\text{Vs}$  as the sulfurization temperature further increases to 580 °C. The decreasing and further increasing trend of the mobility with temperature can be attributed to the effects of acoustic phonon scattering, and scattering by the ionized impurities, respectively. Resistivity of sample T1 is the lowest among all samples. The formation of Sn-rich  $\text{Cu}_4\text{Sn}_7\text{S}_{16}$  and lower crystallinity are responsible for this lower resistivity. However, this value increases accordingly with sulfurization temperature, which can be attributed to the vanishing of this secondary phase and better crystallinity at higher temperature. In this study, higher sulfurization temperature has been found to improve the semiconducting properties of CTS thin films.

Table 2. Electrical properties of sulfurized CTS thin films at different temperatures.

Sample	Carrier Concentration ( $\text{cm}^{-3}$ )	Mobility ( $\text{cm}^2/\text{Vs}$ )	Resistivity ( $\Omega\text{-cm}$ )
T1	1.11E+18	1.14	4.93
T2	5.09E+17	1.07	11.51
T3	1.44E+17	3.60	14.83

#### 4. Conclusions

The CTS thin films were prepared by sputtering deposition followed by subsequent sulfurization at different temperatures. Influence of sulfurization temperature on the structural, morphological, optical, and electrical characteristics of CTS thin films was investigated in this study. The fabricated films were identified as the monoclinic CTS phase with (-131) preferred orientation. Secondary phase,  $\text{Cu}_4\text{Sn}_7\text{S}_{16}$  produced at lower temperature and disappeared gradually as the temperature increased while  $\text{Sn}_2\text{S}_3$  emerged as the secondary phase.

Measurement of Cu/Sn, S/metal ratio signified that Sn, and S were lost accordingly as the sulfurization temperature increased. Grain size was found to increase with higher temperature, suggesting better crystallinity at higher sulfurization temperature. Direct optical bandgap of these thin films was measured from 0.87 eV to 0.92 eV with increasing temperature. Carrier concentration showed a decreasing trend from 1.11E+18 to 1.44E+17 with increasing temperature, while mobility and resistivity were found to follow an increasing trend. From this study, 580 °C was found as the optimum sulfurization temperature for the CTS films.

#### Acknowledgements

The findings achieved herein are solely the responsibility of the authors. The authors would like to acknowledge and appreciate part of the contribution from UKM through research grant GUP-2017-031.

#### References

- [1] A. Green Martin, Y. Hishikawa, D. Dunlop Ewan, H. Levi Dean, J. Hohl-Ebinger,

- W. Y. Ho-Baillie Anita, *Progress in Photovoltaics: Research and Applications* **26**(7), 427 (2018).
- [2] C. Candelise, J. F. Speirs, R. J. K. Gross, *Renewable and Sustainable Energy Reviews* **15**(9), 4972 (2011).
- [3] W. Wang, T. Winkler Mark, O. Gunawan, T. Gokmen, K. Todorov Teodor, Y. Zhu, B. Mitzi David, *Advanced Energy Materials* **4**(7), 1301465 (2013).
- [4] S. Chen, X. G. Gong, A. Walsh, S.-H. Wei, *Applied Physics Letters* **96**(2), 021902 (2010).
- [5] A. Nagoya, R. Asahi, R. Wahl, G. Kresse, *Physical Review B* **81**(11), 113202 (2010).
- [6] M. Bouaziz, M. Amlouk, S. Belgacem, *Thin Solid Films* **517**(7), 2527 (2009).
- [7] P. A. Fernandes, P. M. P. Salomé, A. F. D. Cunha, *Journal of Physics D: Applied Physics* **43**(21), 215403 (2010).
- [8] M. Bouaziz, J. Ouerfelli, S. K. Srivastava, J. C. Bernède, M. Amlouk, *Vacuum*, **85**(8), 783 (2011).
- [9] Y.-T. Zhai, S. Chen, J.-H. Yang, H.-J. Xiang, X.-G. Gong, A. Walsh, J. Kang, S.-H. Wei, *Physical Review B* **84**(7), 075213 (2011).
- [10] P. Zawadzki, L. L. Baranowski, H. Peng, E. S. Toberer, D. S. Ginley, W. Tumas, A. Zakutayev, S. Lany, *Applied Physics Letters* **103**(25), 253902 (2013).
- [11] S. Sato, H. Sumi, G. Shi, M. Sugiyama, *Physica Status Solidi (c)* **12** (2015).
- [12] K. Chino, J. Koike, S. Eguchi, H. Araki, R. Nakamura, K. Jimbo, H. Katagiri, **51** (2012).
- [13] A. Naoya, K. Ayaka, K. Kazuki, Y. Manami, T. Kotoba, A. Hideaki, T. Akiko, K. Hironori, *Japanese Journal of Applied Physics* **53**(5S1), 05FW13 (2014).
- [14] Z. Tang, K. Kosaka, H. Uegaki, J. Chantana, Y. Nukui, D. Hironiwa, T. Minemoto, *Physica Status Solidi (a)*, **212**(10), 2289 (2015).
- [15] K. Junpei, C. Kotaro, A. Naoya, A. Hideaki, N. Ryota, J. Kazuo, K. Hironori, *Japanese Journal of Applied Physics* **51**(10S), 10NC34 (2012).
- [16] A. Mehdi, M. Mohamad Mehdi Bagheri, E. Hosein, *Physica Scripta* **85**(3), 035603 (2012).
- [17] Z. Su, K. Sun, Z. Han, F. Liu, Y. Lai, J. L. Y. Liu, Fabrication of ternary Cu–Sn–S sulfides by a modified successive ionic layer adsorption and reaction (SILAR) method, 2012.
- [18] I. Naji, M. Alias, B. Taher, A. Al-Douri, *Chalcogenide Letters* **15**(2), 83 (2018).
- [19] D. Tiwari, T. K. Chaudhuri, T. Shripathi, U. Deshpande, *Journal of Physics and Chemistry of Solids* **75**(3), 410 (2014).
- [20] N. Mitsuki, F. Junya, Y. Toshiyuki, I. Masanobu, *Applied Physics Express* **8**(4), 042303 (2015).
- [21] N. G. Renganathan, M. V. Subramanian, S. Mohan, *International Journal of Engineering, Science and Technology* **3**(1), 206 (2011).
- [22] R. Chierchia, F. Pigna, M. Valentini, C. Malerba, E. Salza, P. Mangiapane, T. Polichetti, A. Mittiga, *Physica Status Solidi C* **13**(1), 35 (2015).
- [23] Z. Zaihasraf, C. Puvaneswaran, R. Mohammad Junaebur, A. Md, A. Mohammad Mezbau, A.-O. Zeid Abdullah, A. Abdulrahman, S. Kamaruzzaman, A. Nowshad, *Japanese Journal of Applied Physics* **54**(8S1), 08KC18 (2015).
- [24] M. Onoda, X.-A. Chen, A. Sato, H. Wada, *Materials Research Bulletin* **35**(9), 1563 (2000).
- [25] D. M. Berg, R. Djemour, L. Gütay, G. Zoppi, S. Siebentritt, P. J. Dale, *Thin Solid Films* **520**(19), 6291 (2012).
- [26] H. Guan, H. Shen, C. Gao, X. He, *Journal of Materials Science Materials in*

- Electronics **24**(5) (2012).
- [27] P. Zhao, S. Cheng, *Advances in Materials Science and Engineering*, **2013** (2013).
- [28] Y. Dong, J. He, L. Sun, Y. Chen, P. Yang, J. Chu, *Materials Science in Semiconductor Processing* **38**, 171 (2015).
- [29] P.-W. Guan, S.-L. Shang, G. Lindwall, T. Anderson, Z.-K. Liu, *Solar Energy* **155**, 745 (2017).
- [30] P. Chelvanathan, Z. Zakaria, Y. Yusoff, M. Akhtaruzzaman, M. M. Alam, M. A. Alghoul, K. Sopian, N. Amin, *Applied Surface Science* **334**, 129 (2015).
- [31] P. Chelvanathan, S.A. Shahahmadi, F. Arith, K. Sobayel, M. Akhtaruzzaman, K. Sopian, F.H. Alharbi, N. Tabet, N. Amin, *Thin Solid Films* **638**, 213 (2017).
- [32] F. Jiang, S. Ikeda, T. Harada, M. Matsumura, *Advanced Energy Materials* **4**(7), 1301381 (2013).
- [33] S. Ahmed, B. Reuter Kathleen, O. Gunawan, L. Guo, T. Romankiw Lubomyr, H. Deligianni, *Advanced Energy Materials* **2**(2), 253 (2011).
- [34] L. Guo, Y. Zhu, O. Gunawan, T. Gokmen, R. Deline Vaughn, S. Ahmed, T. Romankiw Lubomyr, H. Deligianni, *Progress in Photovoltaics: Research and Applications* **22**(1), 58 (2013).
- [35] Y. Lin, S. Ikeda, W. Septina, Y. Kawasaki, T. Harada, M. Matsumura, *Solar Energy Materials and Solar Cells* **120**, 218 (2014).
- [36] M. M. I. Sapeli, M. T. Ferdaous, S. A. Shahahmadi, K. Sopian, P. Chelvanathan, N. Amin, *Materials Letters* **221**, 22 (2018).
- [37] U. Chalapathi, B. Poornaprakash, S. H. Park, *Chalcogenide Letters* **13**(7), 325 (2016).
- [38] L. Yang, B. Kruse, *J. Opt. Soc. Am. A Opt. Image Sci. Vis.* **21**(10), 1933 (2004).
- [39] U. Chalapathi, Y. Jayasree, S. Uthanna, V. Sundara Raja, *Vacuum*, **117**, 121 (2015).
- [40] A. Kanai, H. Araki, A. Takeuchi, H. Katagiri, *Physica Status Solidi (B)* **252**(6), 1239 (2015).
- [41] Y. Miyata, S. Nakamura, Y. Akaki, *Physica Status Solidi C*, **12**(6), 765 (2015).
- [42] E. S. Hossain, P. Chelvanathan, S. A. Shahahmadi, K. Sopian, B. Bais, N. Amin, *Current Applied Physics* **18**(1), 79 (2018).
- [43] O. V. Emelyanenko, T. S. Lagunova, D. N. Lagunova, G. N. Talalakin, *Soviet Physics, Solid State* **7**, 1063 (1965).
- [44] G. Marcano, C. Rincón, L. M. de Chalbaud, D. B. Bracho, G. S. Pérez, *Journal of Applied Physics* **90**(4), 1847 (2001).